

Design Analysis and Performance testing of a Novel Passive Thermal Management System for Future Exploration Missions

Angel R. Alvarez-Hernandez and Stephania Ortega
NASA Johnson Space Center, Houston, TX 77058, USA

Jeffery T. Farmer and Shawn Breeding
NASA Marshall Space Flight Center, Huntsville, AL 35808, USA

Calin Tarau, Mohammed T. Ababneh, and William G. Anderson
Advanced Cooling Technologies, Inc., 1046 New Holland Ave., Lancaster, PA 17601, USA

In response to an announcement of opportunity from NASA’s Science Mission Directorate (SMD) Discovery Program, the Southwest Research Institute in collaboration with the Aerospace Corporation and the NASA Johnson Space Center (JSC) proposed a lunar lander science mission. The Moon Age and Regolith Explorer (MARE) would use a lunar lander to reach a young, nearside lunar lava flow for the collection and analysis of the lunar soil. This would be used for the determination of the impact history of the inner solar system and the evolution and differentiation of the interiors of one-plate planets. The lunar lander proposed was based on the NASA JSC Morpheus lander vehicle. The thermal environments for the proposed mission were both challenging and unprecedented, since survival of multiple lunar day/night cycles at the south-west region of the Aristarchus plateau were required. Other thermal design challenges included the need for a low mass, robust and reliable thermal management system that would assure the success of the proposed mission. As part of the proposal effort, and leveraging on existing NASA Small Business Innovative Research (SBIR), a completely passive thermal control system concept was used to meet mission requirements. The thermal management system proposed uses a novel type of hybrid grooved and sintered wick variable conductance heat pipe and a high conductivity heat spreader; the thermal management systems tested were developed by Advanced Cooling Technologies, Inc. (ACT) in Lancaster, Pennsylvania. This publication will present the design, analysis and prototype component and system level performance testing done at NASA JSC.

Nomenclature

ACT	=	Advanced Cooling Technologies, Inc.	MARE	=	the Moon Age and Regolith Explorer
APG	=	Annealed Pyrolytic Graphite	NCG	=	Non Condensable Gas
APT _x	=	Advanced Passive Thermal experiment	NESC	=	NASA Engineering and Safety Center
CCHPs	=	Constant Conductance Heat Pipes	SBIR	=	Small Business Innovation Research
C&DH	=	Command and Data Handling	SMD	=	NASA’s Science Mission Directorate
ISS	=	International Space Station	VCHPs	=	Variable Conductance Heat Pipes
JSC	=	Johnson Space Center			

I. Introduction

In this work, there will be some differences between the MARE thermal control system design proposed and the actual test article built and tested. The end goal of the effort remains the same: the proof of concept of a completely passive thermal management system for a mid-sized lunar lander spacecraft. This effort also addressed technical gaps identified in the NASA technology roadmaps ^[1]. In this paper and per the definition of the NASA Engineering and Safety Center (NESC) Passive Thermal Discipline, the authors define a passive system as an architecture without the use of a mechanically pumped fluid loop. This effort, led by the NASA Johnson Space Center’s (JSC) Passive Thermal Technical Discipline Lead (TDL) and the Technology Development team in the thermal design

branch, had an additional objective; to demonstrate an initiative to reduce cost and infuse existing research into needed NASA applications by leveraging on existing Small Business Innovation Research (SBIR) contracts. A variation of the hybrid wick VCHP and the high conductivity, HiK™, plates used in this work were also tested in the ISS as part of the technology experiment suite, under the JSC Advanced Passive Thermal experiment project [2] [3] [4].

The MARE (Moon Age and Regolith Explorer) Discovery Mission concept targets delivery of a science payload to the lunar surface for sample collection and dating with the objective of determining the impact history of the inner solar system and the evolution and differentiation of the interiors of one-plate planets. The mission science is within a 100-meter radius region of smooth lunar maria terrain near Aristarchus crater, 23.7°N 47.4°W . The lunar lander proposed for this mission was based on the NASA JSC Morpheus lander vehicle.



Figure 1: MARE Lander Configuration

As part of this work, the NASA JSC and MSFC thermal teams proposed a thermal management system. This thermal management concept was intended to not only meet the driving requirements below, but also leverage on existing SBIR work with the objective of developing technologies that have the potential of reducing mass, power, cost and complexity while maintaining thermal performance for future architectures.

- The science payload should be able to survive approximately 2 lunar days and one lunar night.
- The thermal control system should be able to dissipate 323 watts of waste heat during science payload operations.
- Thermal control should be able to keep all components within operational and survival limits for science payloads and lander components for extended periods of time.
- The thermal control system should be able to operate during different mission phases.
- The thermal control system should be able to operate at a 25° slope.

The design approach took into consideration the following thermal control strategy in order to propose a simplified thermal management solution for this mission.

- Passive thermal control will be pursued to the extent possible to reduce complexity, mass and cost.
- Package components to be thermally conditioned in one location if possible.
- Assume payload structure is thermally optimized to be controlled by a common heat spreader.
- Passive heat spreader plate
 - Controlled to a set temperature range (0°C to 50°C) via heat pipes and heaters.
 - Directly mount multiple subsystem components to the top side of the heat spreader plate, (two sided heat spreader could be an option),

- Structure must be thermally isolated from heat spreader to control heat leaks. (the use of heat switches can be evaluated)
- Use of variable conductance heat pipes to thermally connect to the radiator.
- MLI will be used to cover the exterior surface of the thermal control system to protect from environment.
- Remote units will be evaluated separately and proper thermal controls will be placed.
- Heater will be used to survive lunar night.

The thermal math modeling performed during the analysis iterations followed the below stated assumptions.

- Components to be controlled are located in the same thermal control area (on heat spreader).
- All components are covered with MLI boxes. Assumed value $\epsilon^* = .03$.
- Radiators are tilted to avoid view to the lunar surface and assuming a full view to space.
- Radiators are protected from lunar dust during landing.
- Radiators have a low α/ϵ coating such as white paint Z93 or silver Teflon .
- Payload and lander component total peak thermal load assumed to be 323 watts.
- Battery operational limits assumed to be $0^\circ - 50^\circ\text{C}$.
- Payload and Morpheus components survival low temperature limit assumed -10°C .
- All components will shutdown for the lunar night, with only the heaters active.

II. Proposed Thermal Design

The MARE thermal control system (TCS) design proposed is intended to ensure that all spacecraft and science components are maintained within operational/survival limits throughout all mission phases. The lunar surface operation phase presents the most challenging thermal environment for heat rejection given the imposed thermal loads and heat rejection sink temperatures. Lunar surface temperatures can vary drastically and range from -173°C at lunar night to 87°C during lunar day. In addition, the long-duration, cold, lunar night drives heater power requirements to keep components within their temperature limits. The MARE thermal control architecture proposed consists of a simple passive thermal control system, making this a reliable, cost and mass-effective approach. This system is composed of two thermally controlled zones on the top deck of the spacecraft to maintain science and vehicle components within operational and survival limits. Cooling is achieved with two high conductivity heat spreaders connected via hybrid Variable Conductance Heat Pipes (VCHPs) [5] [6] to two high conductivity radiators. In the proposal phase, two high conductivity aluminum encapsulated Annealed Pyrolytic Graphite (APG) heat spreaders were assumed as the heat spreader plate and the radiators. Driven by cost reduction, and the opportunity to leverage on existing SBIR contracts, these were replaced for testing for 2 HiK™ plate heat spreaders, one HiK™ plate radiator and one Gas Charged Heat Pipe (GCHP) radiator. The thermal links provide a means to control the heat leak from the heat spreaders, depending on the set-point. They conduct heat to the radiators when the heat spreader surface temperature is above the upper temperature limit and turn off by heating the non-condensable gas reservoir, disconnecting the ammonia flow within the VCHP, when the heat spreaders are below the lower temperature limit. Figures 2 and 3 shows the original thermal management concept and technical definitions presented during the proposal.

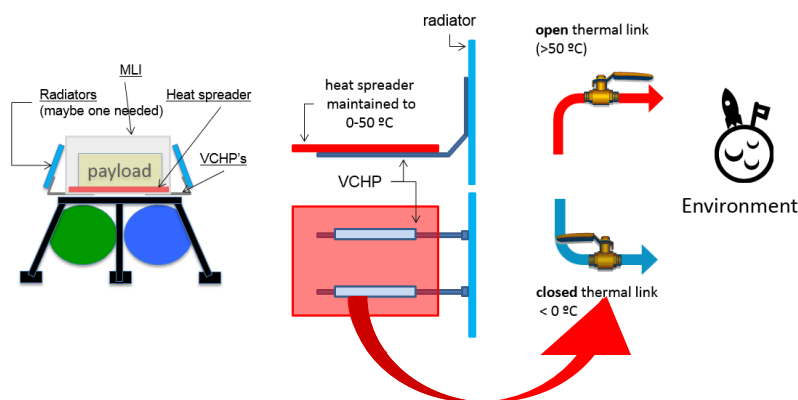


Figure 2: MARE Thermal Concept

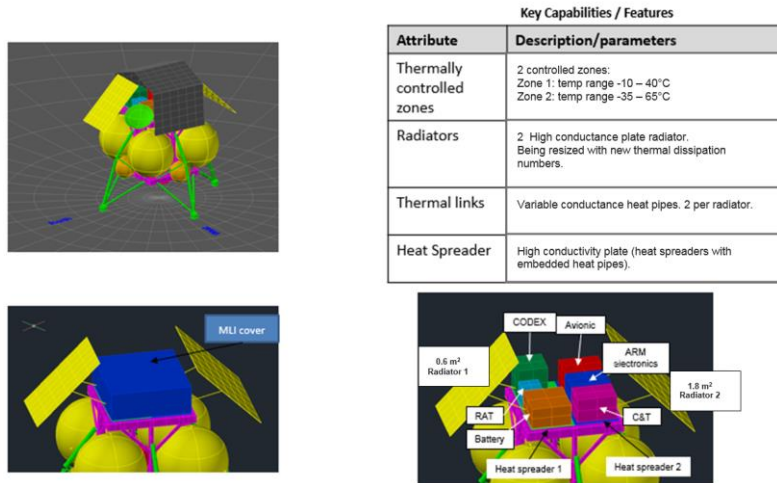


Figure 3: MARE Thermal Concept Description

As part of the lunar operations power requirements, the vehicle would land with both radiators perpendicular to the sun angle. The radiators proposed assumed an AZ-93 surface coating with solar absorptivity/emissivity of 0.19/0.89 to reduce the amount of incident thermal load and to reject heat in the infrared spectrum. An assessment of dust degradation was not included and the effects were expected to be covered with the design margin. The lunar surface IR thermal load on the radiator is minimized by positioning the radiators at a 45° angle from the local vertical. The first radiator is 0.6 m² and is located on the south facing side of the spacecraft. This radiator rejects a maximum waste heat of 88W produced by zone 1 (CDEX, RAT and batteries) as shown in figure 3. The second radiator is 1.8m² and is located on the north facing side of the spacecraft. This radiator rejects a maximum waste heat of 235 watts produced by the spacecraft avionics, telecom and lander electronics in zone 2.

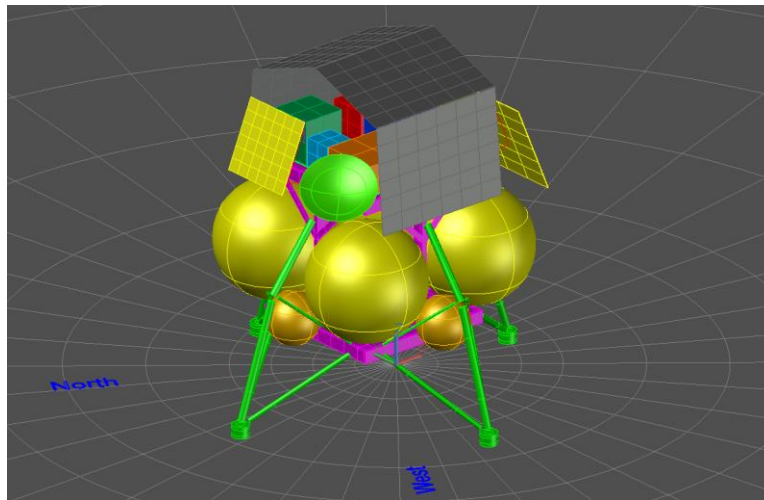


Figure 4: MARE Thermal Math Model

In order to survive the lunar night, thermostatically controlled Kapton heaters, directly fed from the primary battery input, provide the necessary heat to keep electrical components within operational and survival thermal limits. The survival heater power needed is approximately 55 watts. Multi-Layered Insulation (MLI) blankets will shroud all top deck components to reduce the amount of heat leak paths to the cold lunar environment and space environment. A thermal math model was developed for the proposed MARE TCS architecture, and thermal analysis was performed for the worst cold and hot mission environments. The results show that the TCS subsystem will protect the MARE payload from worst case hot mission environment with at least a 13°C margin for all components. Results also showed at least 12°C margin for all components for a worst case cold mission environment.

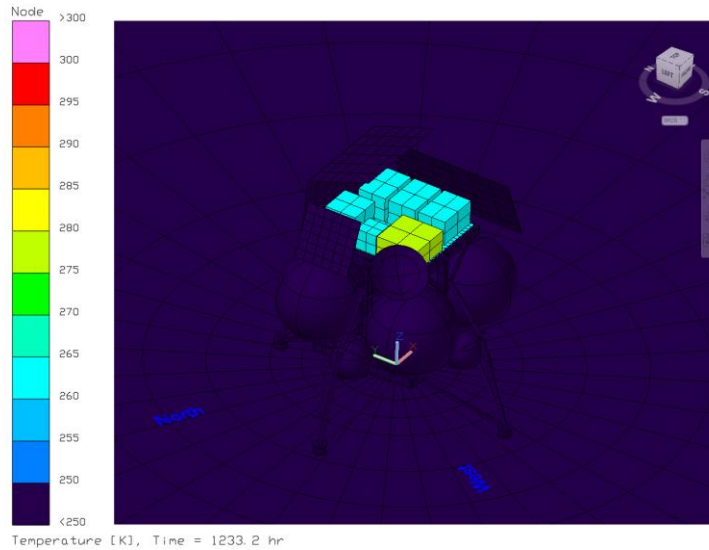


Figure 5: Thermal analysis showing all components above their lower operational limits during lunar night.

HEALTHY THERMAL MARGINS WITH 0.6 m ² AND 1.8 m ² RADIATORS										
Temp (°C)	Survival Limits		Operational Limits		High Limit	Hot Pred.	Hot Margin	Low Limit	Low Pred.	Low Margin
	Low	High	Low	High						
CDEX	-55	70	-20	50	50	37	13	-55	-21	34
Battery	-50	60	-10	50	50	37	13	-10	2	12
C&DH	-50	70	-35	60	60	35	25	-50	-25	25
SSG	-55	70	-40	85	85	39	46	-55	-15	40
Telecom	-55	85	-35	71	71	35	36	-55	-25	30
Arm Elect.	-50	80	-40	70	70	34	36	-50	-25	25

Figure 6: Analysis summary of all components during their worst case thermal environments.

III. Thermal Management Components

After the proposal phase, the thermal management concept was further defined, including the system interfaces, in order to pursue the integrated thermal vacuum testing. The heat spreader required a structurally sound and thermally insulating interface to the vehicle structure to minimize conductive losses. The entire system required Multi-Layer Insulation (MLI) to reduce the radiative heat loss to the environment. Finally thermal interface materials were selected to attach the three main components of the thermal control system, heat spreader plates, thermal links and radiators.

The thermal control system is thermally insulated from the frame using the thermal spacers and insulated from the environment using a custom Multi-Layer Insulation (MLI) system.

Thermal spacers

A novel approach to optimizing the tradeoff between strength and low thermal conductivity was to additively manufacture the thermal spacers connecting the heat spreader to the vehicle structure. No details of the thermal spacers can be provided at the moment of this publication.

MLI

A custom MLI system was designed to minimize radiative heat losses to the environment during testing. This MLI system was intended to be as close to a flight product as possible, given the material and budget available. Note that some of the materials used in the MLI stackup were simply used given their availability. The system fully enclosed

the heat spreader, thermal link, and back face of the radiator. The design included Velcro for easy removal and adjustability. Each piece of the MLI was constructed using Aluminized Mylar, Dacron netting, nylon thread, and Velcro. The stackup and pattern for the MLI are shown below. Figure 7 shows how the MLI system was installed for one test article configuration. Figure 8 shows the MLI configuration for the heat spreader while Figure 9 shows the stackup for the heat spreader. The MLI was manufactured at JSC by the Passive Thermal Technology development team for thermal vacuum testing purposes.

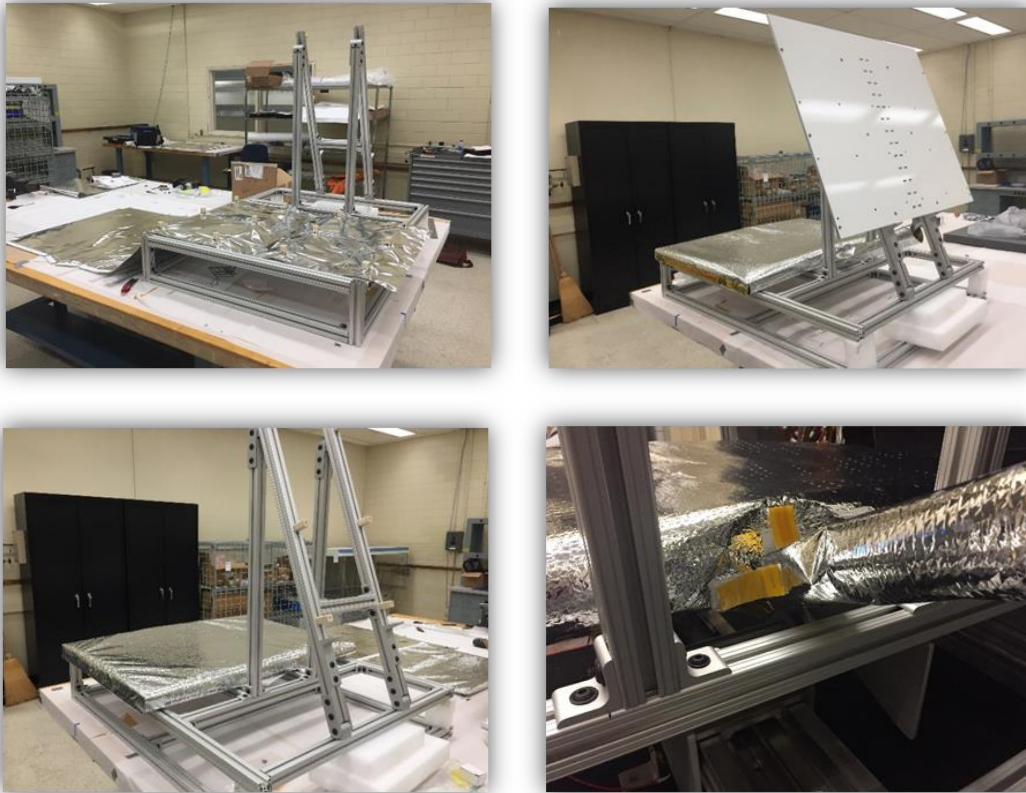


Figure 7: MLI assembly

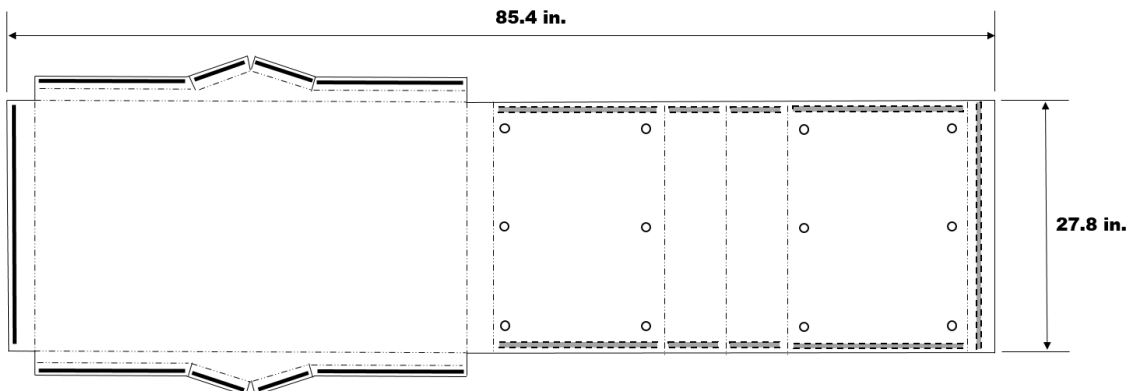


Figure 8: MLI configuration for heat spreader

MLI Construction	
Layer	Material
1 (Outer)	Al-My 0.5 mil w/ integrated scrim
2	Al-My 1.0 mil
	Dacron netting
3	Al-My 0.5 mil w/ integrated scrim
4	Al-My 1.0 mil
	Dacron netting
5	Al-My 0.5mil w/ integrated scrim
6	Al-My 1.0 mil
	Dacron netting
7	Al-My 0.5 mil w/ integrated scrim
8	Al-My 1.0 mil
	Dacron netting
9	Al-My 0.5 mil w/ integrated scrim
10 (Inner)	Al-My 1.0 mil

Figure 9: MLI layout

Thermal Interface Material

To reduce resistance throughout the passive thermal control system assembly, Tgon 800 series was selected as the thermal interface material. This thin piece of graphite is lightweight, low outgassing, and has a high in plane conductivity of 240 W/mK.

All of these components were incorporated into the test articles to demonstrate system performance during thermal vacuum test.

HiK™ Plates

A heat spreader is a high conductivity plate used to isothermize the vehicle electronics and payload. For this effort the team was able to leverage off of an existing SBIR to procure, at a lower cost compared to any other option in the market, HiK™ plates from Advanced Cooling Technologies, Inc. HiK™ plates are a novel passive thermal design that incorporate constant conductance heat pipes embedded in a core aluminum structure. This results in an increase in in-plane thermal conductivity while decreasing mass compared to other cold plate or heat spreader systems. The manufacturing approach used for the HiK™ plates make this an affordable and tailorable option for other thermal management systems. By the time this publication was completed, the HiK™ plates were tested inside the ISS as part of the JSC Passive Thermal Development initiative. The APTx payload testing included freeze/thaw cycles in a microgravity environment resulting in no performance and hardware degradations [3].

Thermal Links

A thermal link transfers the heat from the heat spreader to the radiator. Two thermal links were evaluated in this test: a Constant Conductance Heat Pipe (CCHP) as a baseline design and a novel Variable Conductance Heat Pipe (VCHP). This CCHP is a dual bore, groove wicked system, designed to transport at least 150W. The VCHP has a hybrid wick and warm biased reservoir. The hybrid wick combines a sintered evaporator wick to handle high heat fluxes and an increased capillary force to improve performance against gravity, with an axially grooved adiabatic and condenser section to transfer heat over long distances. The warm biased reservoir reduces the amount of auxiliary heating compared to standard, cold-biased reservoir VCHPs. In addition, the integrated design reduces the overall footprint of the evaporator portion. The reservoir of the non-condensable gas (NCG) allows for shutdown, the state when the gas has expanded to reduce the overall effective length of the heat pipe to just beyond the evaporator portion, and isolates the radiator from the heat spreader. Both integrated reservoir and hybrid-wick concepts were tested as part of the APTx suite of experiments [4]. Improvement to the integrated reservoir design are currently in work.

Radiators

A radiator rejects the heat transferred from the thermal link to the environment. Two types of radiators were included in this evaluation: a HiK™ and Gas Charged Heat Pipe (GCHP). The HiK™ radiator includes the same internal design as a HiK™ heat spreader. The Gas Charged Heat Pipe Radiator consisted of six GCHPs mounted to

an aluminum plate. These GCHP's have a gas charged reservoir. Changing of the boundary temperature and incoming power reduces the vapor pressure of the working fluid, allowing the gas to either expand or contract at the newly equalized pressure. The expansion of the gas changes the overall effective length of the heat pipe, and therefore the amount of heat transferred. This allows for shutdown at a radiator level, isolating the radiator from the thermal link. Both radiators had the same high emissivity coating with a total hemispherical emissivity of 0.8. In order to remain within budget constraints, the radiators were sized for different loads. Given the complexity of the GCHP radiator, the largest size that the project could afford had a front radiative area of 0.368m²; the HiK™ radiator had a front radiative area of 0.697m².

IV. Testing

Four configurations were tested, each comprised of a unique combination of heat spreader, thermal link, and radiator. Two systems were evaluated simultaneously for each test case.

Configurations

The four configurations are listed below in Table 1.

Table 1: Testing Configurations

Configuration	Heat Spreader	Heat Pipe	Radiator
1	HiK™	CCHP	HiK™
2	HiK™	VHCP	GCHP
3	HiK™	CCHP	GCHP
4	HiK™	VCHP	HiK™

Configuration 1 was determined to be the baseline design; Configuration 2 was the novel design. Configurations 3 and 4 allowed the shutdown to be evaluated for the VCHP and GCHP independently.

Test Setup

Chamber Configuration

Testing was conducted in Chamber E at the Johnson Space Center. The chamber maintained a pressure of less than 1 X 10⁻⁴ torr and a shroud temperature of -172°C. The final test configuration included a multilayered mylar wall separating the two test articles in order to minimize radiative heat transfer between the two systems.

Mechanism

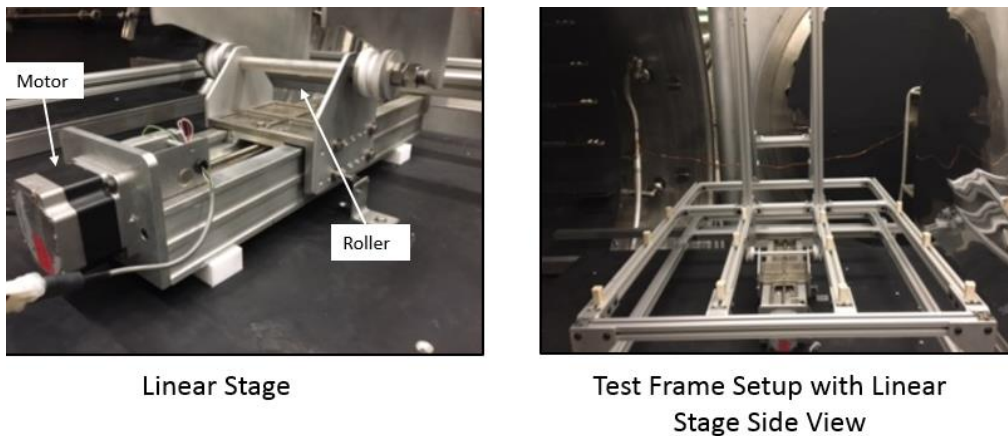


Figure 10: Testing motor and mechanism

Each test configuration was fixed to an 80-20 Aluminum frame. This frame held the test articles in place and provided additional support for the radiator to alleviate the force applied to the thermal link. The frame was in turn mounted onto a linear stage actuator with a motor to change the angle of inclination of the test articles. The system could be adjusted $\pm 4.2^\circ$ from 0° to account for a vehicle design requirement to maintain performance at $\pm 25^\circ$ on the lunar surface. The entire assembly was bolted to a table on rails that could be pulled out from the chamber to ease installation and assembly. The test articles were attached to the frame using thermal spacers.



Figure 11: Test article configuration in the chamber (back)

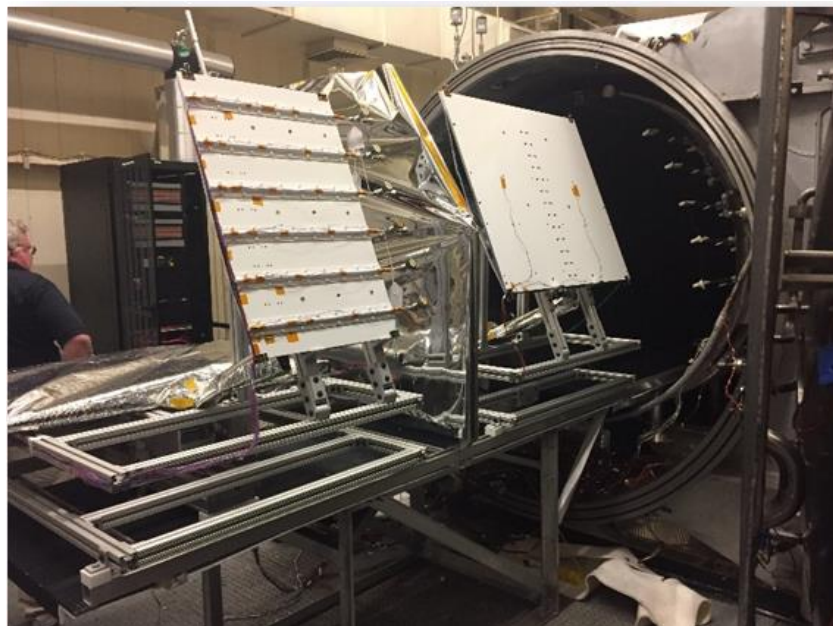
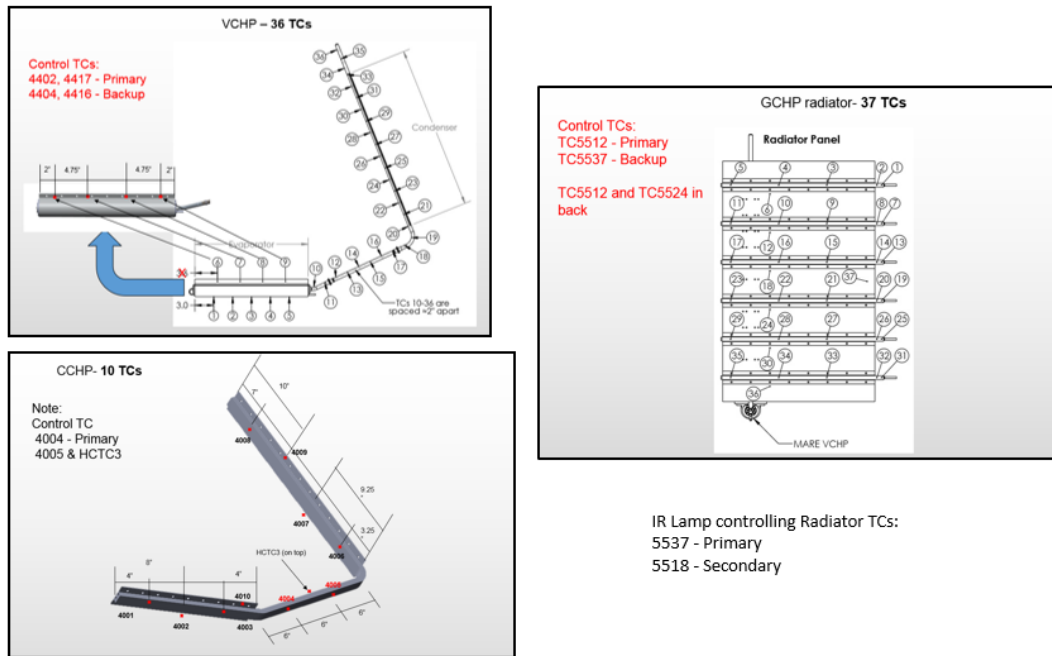


Figure 12: Test article configuration in the chamber (front)

TC Maps

The test used 118 facility provided Type T thermocouples to evaluate thermal performance of the system.

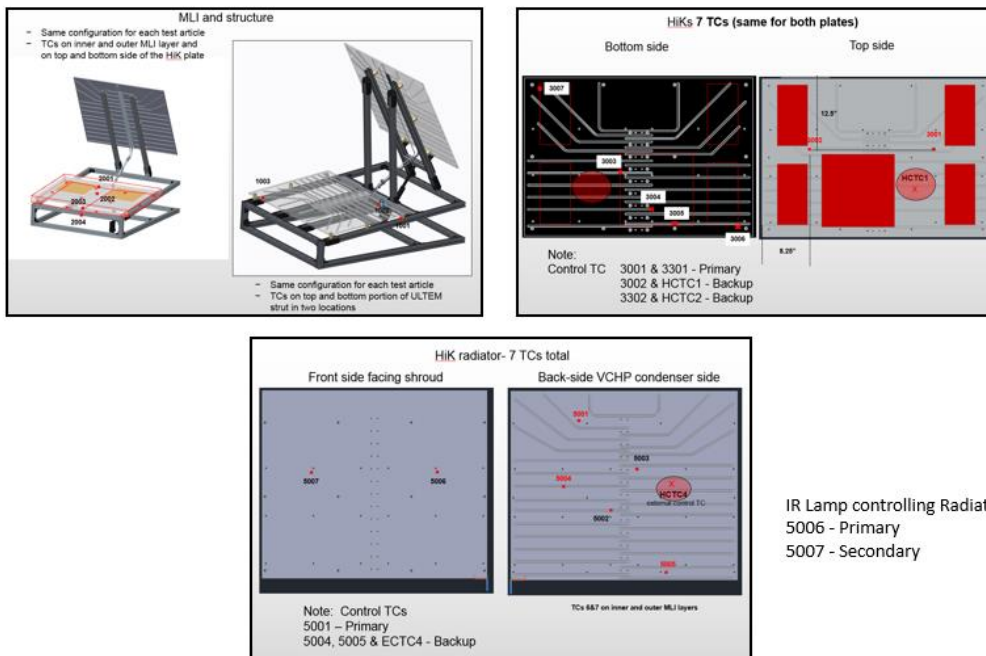
The layout of the thermocouples can be seen in the images below.



IR Lamp controlling Radiator TCs:
5537 - Primary
5518 - Secondary

Figure 13: VCHP, CCHP and GCHP radiator TC map.

Thermocouples were added to the frame to characterize heat leak through the thermal spacers, internal and external MLI surfaces to quantify the effectiveness of the MLI system, and to the HiK™ plates, thermal links, and radiators. The VCHP and GCHP radiator had the most thermocouples to monitor where the vapor-gas front was during thermal control and survival testing.



IR Lamp controlling Radiator TCs:
5006 - Primary
5007 - Secondary

Figure 14: MLI, HiK™ heat spreader and HiK™ plate radiator TC map.

Heater Map

Twenty-two Kapton heaters and one rope heater were used to provide the boundary conditions for the test systems.

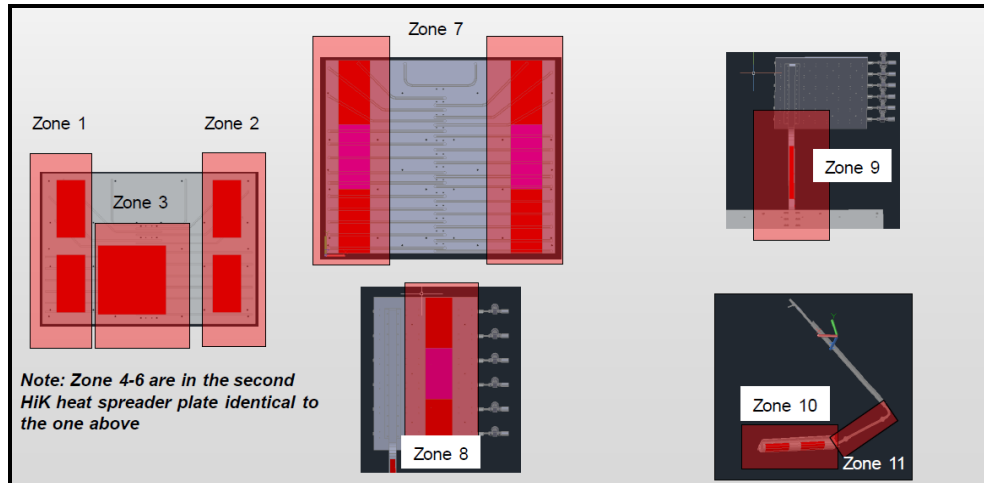


Figure 15: Heater Map

These heaters were separated into 11 zones, each controlled by a pulse width modulation (PWM) system of NI DAQ system, Solid State Relays (SSR), and power supplies.

Controls

The heating system was controlled using a NI 9472 Digital I/O card, Crydom SSR's and power supplies from Omega and BK Precision. The LabView program had options to control to a power or a temperature and recorded the average power being applied to the hardware.

The power supplies were each set to a maximum output power per zone, as shown below in Table 2.

Table 2: Maximum power per heater zone

Zone	1	2	3	4	5	6	7	8	9	10	11
Power (Watts)	192	191	281	188	191	292	380	193	97	144	90

The Q_{in} and $Q_{in_Radiator}$ was calculated by the LabView program multiplying the duty cycle sent to the SSR by the maximum power measured. The system could be controlled to a power by inputting a duty cycle that corresponded to the desired power. The system could be controlled to a temperature using a simple control loop that turned the power on if the control temperature was below the desired temperature and turned the system off if the control temperature was above the desired temperature. The system calculated a duty cycle from this on/off pulsing and multiplied by the maximum measured power.

Test Plan

Tests to characterize thermal control and survival were completed for all test configurations. Configurations 1 and 2 also evaluated the maximum heat transport for given conditions. Due to the time available, not all tests could be performed for all four configurations. The test matrix is shown below. Test Cases 1 and 7 were controlled to the heat spreader temperature design limits. Though the MARE lander was designed for operation from 0 to 50°C, these configurations were designed for operation from 0 to 60°C to accommodate other landers' design requirements at the time. Test Cases 2 through 6 were controlled to a constant power on the heat spreader, simulating component loads, while the radiator surface temperature was changed to verify performance of the system. Cases 2 through 6 demonstrate the variable transport capability of the VCHP and GCHP radiator.

Table 3: Test matrix

Test Case	Heat Spreader Control	Radiator Control	Configuration Tested			
			1 (CCHP, HiK™)	2 (VCHP,GCHP)	3 (CCHP,GCHP)	4 (VCHP, HiK™)
1	50°C	N/A	X	X	-	-
2	150W	Hot	X	X	X	X
3	150W	20°C	X	X	X	X
4	150W	10°C	X	X	X	X
5	150W	N/A	X	X	X	X
6	100W	N/A	X	X	X	X
7	0°C	N/A	X	X	X	X

V. Results

The steady state temperature data for each test case is summarized below; steady state was defined by a change of less than 2°C per half hour.

Table 4a: Temperature data – Configuration 1

Configuration 1	Test Case						
	1	2	3	4	5	6	7
	Average Temperature (°C)						
HiK™ Radiator Out	13	19	6	-3	-19	-39	-44
HiK™ Radiator In	30	36	21	11	-6	-27	-31
HiK™ Plate 1	47	47	32	24	11	-4	-6
CCHP Evaporator	40	43	27	18	1	-21	-25
CCHP Condenser	37	41	25	15	-1	-22	-26
Structure	-99	-93	-98	-102	-108	-114	-125
MLI Top External	-118	-118	-122	-125	-129	-134	-138
MLI Bottom External	-73	-85	-92	-97	-103	-110	-118
MLI Top Internal	40	41	27	18	5	-14	-17
MLI Bottom Internal	32	33	19	11	-2	-16	-21
Environment	-173	-172	-172	-172	-172	-173	-171

Table 4b: Temperature data – Configuration2

Configuration 2	Test Case						
	1	2	3	4	5	6	7
	Average Temperature (°C)						
GCHP Radiator Out	-30	30	21	13	9	-15	-126
GCHP Radiator In	-31	40	29	21	16	-13	-125
HiK™ Plate 2	49	62	60	60	59	52	-1
VCHP Evaporator	46	57	55	54	54	49	-2
VCHP Condenser	-27	41	30	22	17	-8	-126
Structure	-96	-89	-93	-96	-100	-104	-120
MLI Top External	-110	-106	-107	-109	-110	-112	-120
MLI Bottom External	-108	-97	-101	-105	-109	-113	-127
MLI Top Internal	43	58	57	56	55	48	-5
MLI Bottom Internal	30	45	44	42	42	35	-18
Environment	-173	-172	-172	-172	-172	-173	-171

Table 4c: Temperature data – Configuration 3

Configuration 3	Test Case						
	1	2	3	4	5	6	7
	Average Temperature (°C)						
GCHP Radiator Out	N/A	24	14	13	12	-12	-26
GCHP Radiator In	N/A	34	22	21	20	-6	-21
HiK™ Plate 1	N/A	43	33	32	31	6	-4
CCHP Evaporator	N/A	40	29	28	27	-1	-15
CCHP Condenser	N/A	37	26	25	23	-4	-18
Structure	N/A	-68	-90	-97	-102	-110	-132
MLI Top External	N/A	-105	-101	-108	-108	-112	-116
MLI Bottom External	N/A	-51	-72	-78	-84	-94	-103
MLI Top Internal	N/A	38	28	27	26	-1	-14
MLI Bottom Internal	N/A	29	18	17	15	-9	-21
Environment	N/A	-173	-136	-174	-174	-174	-174

Table 4d: Temperature data – Configuration 4

Configuration 4	Test Case						
	1	2	3	4	5	6	7
	Average Temperature (°C)						
HiK™ Radiator Out	N/A	15	3	-6	-33	-56	-143
HiK™ Radiator In	N/A	33	21	12	-17	-42	-143
HiK™ Plate 2	N/A	59	60	59	58	51	-1
VCHP Evaporator	N/A	56	55	54	52	47	-1
VCHP Condenser	N/A	34	23	14	-13	-38	-143
Structure	N/A	-73	-92	-98	-106	-114	-119
MLI Top External	N/A	-118	-110	-123	-129	-133	-143
MLI Bottom External	N/A	-96	-108	-114	-120	-125	-135
MLI Top Internal	N/A	57	57	56	54	48	-5
MLI Bottom Internal	N/A	45	43	42	40	34	-17
Environment	N/A	-173	-136	-174	-174	-174	-174

Calculations

The temperature data was used to calculate the percentage of heat transferred by the thermal control system and the percentage of heat lost to the environment through the MLI system and thermal spacers.

The input load to the system was calculated using the PWM frequency multiplied by the maximum load of the power supply. These calculated loads were used for the rest of the calculations as Q_{in} and $Q_{in_Radiator}$. Q_{in} is the load applied to the heat spreader; $Q_{in_Radiator}$ is the load applied to the radiator.

To evaluate the distribution of each load, the system was analyzed at two control volumes: one at the heat spreader for Q_{in} and one at the radiator for $Q_{in_Radiator}$.

The energy balance at the heat spreader was calculated using the load into the heat spreader, Q_{in} , the heat transferred by the thermal link, and the losses to MLI and Thermal Spacers (TS).

$$Q_{in} = Q_{TCS} + Q_{MLI} + Q_{TS}$$

The energy balance at the radiator was calculated using the loads into the radiator, $Q_{in_Radiator}$ and Q_{TCS} which was calculated above, and the Q_{out} of the radiator. The Q_{out} of the radiator is the sum of the heat radiated from the front face of the radiator and the losses from MLI on the radiator and thermal link and the thermal spacers fixing the radiator. From the data collected, the losses could not be separately calculated and therefore all losses are lumped into $Q_{MLI_Radiator}$.

$$Q_{in_Radiator} + Q_{TCS} = Q_{MLI_Radiator} + Q_{Radiator}$$

Using these two primary equations and the temperature data presented above in Table 4, the system was analyzed to determine the effectiveness of the thermal control system. For the following equations, ϵ is emissivity, σ is the Stefan-Boltzmann constant, A is area, T is temperature, and ϵ^* is effective emissivity.

$$Q_{MLI} = \epsilon_{Plate} * \sigma * A_{Plate} * (T_{Plate}^4 - T_{MLI_Internal}^4)$$

From this Q_{MLI} , an ϵ^* for the heat spreader MLI was back calculated using temperature data on the internal and external faces of the MLI system. The average value for heat spreader MLI was 0.02. This met the design requirement of $\epsilon^* \leq 0.03$. Specific MLI testing will be performed at a later date to confirm these results.

$$Q_{TS} = k_{TS} * A_{TS} / L_{TS} * (T_{Plate} - T_{Structure})$$

$$Q_{TCS} = Q_{in} - Q_{MLI} - Q_{TS}$$

$$Q_{Radiator} = \epsilon_{Radiator} * \sigma * A_{Radiator} * (T_{Radiator}^4 - T_{Boundary}^4)$$

Test Case 1- Maximum Heat Transport

For the first case, the HiK™ plates were maintained to 50°C, the upper limit of the MARE design. The objective of this test was to determine the maximum heat transport capability of the system, comparing the baseline to the novel system. This maximum power is also used to calculate the turn down ratio of the system. Configuration 1 had a maximum power greater than three times that of Configuration 2; this may partially be attributed to the difference in radiator sizing.

Table 5a: Results – Test Case 1

Test Case	1			
Component Q	Configuration			
	1	2	3	4
Q_{in}	295	89	N/A	N/A
$Q_{in_Radiator}$	0	0	N/A	N/A
	Percentage (%)			
Q_{TCS}	95	81	N/A	N/A
Q_{MLI}	4	15	N/A	N/A
Q_{TS}	1	4	N/A	N/A
$Q_{Radiator}$	79	83	N/A	N/A
$Q_{MLI_Radiator}$	21	17	N/A	N/A

Test Case 2 - Maximum Sink for 150 watts

For Case 2, 150W was input to the heat spreader continuously and the radiator temperatures were adjusted until the vapor reference node in the VCHP reached 50°C. The objective of this test was to determine the state in which the VCHP was designed to be fully open, or all of the Non-Condensable Gas was in the reservoir.

Table 5b: Results – Test Case 2

Test Case	2			
Component Q	Configuration			
	1	2	3	4
Q_{in}	150	150	150	150
$Q_{in_Radiator}$	166	47	30	141
	Percentage (%)			
Q_{TCS}	91	90	91	91
Q_{MLI}	7	9	7	6
Q_{TS}	2	2	2	3
$Q_{Radiator}$	80	82	82	82
$Q_{MLI_Radiator}$	20	18	18	18

Test Cases 3 to 6 -Thermal Control

The objective of this test was to characterize the performance of the lander TCS. These tests demonstrate the ability to maintain a heat spreader, or electronics plate, within the design temperature limits, given a range of radiator temperatures and Q_{in} .

In the plots below, HiK™ heat spreader temperature is compared to radiator temperature and Q_{in} power for Cases 2 through 6. Figure 16 shows Configuration 1 compared to 4, demonstrating the effect of the thermal link on a HiK™ heat spreader and HiK™ radiator system. Figure 17 shows Configuration 2 compared to 3, demonstrating the effect of the thermal link on a HiK™ heat spreader and GCHP radiator system. Though Configurations 2, 3, and 4 maintained the heat spreader within design temperature limits, Configurations 2 and 4 that utilized the VCHP as the thermal link provided the tightest temperature control at the heat spreader in Cases 2 through 6 compared to the baseline, Configuration 1, and the GCHP Radiator with the CCHP in Configuration 3.

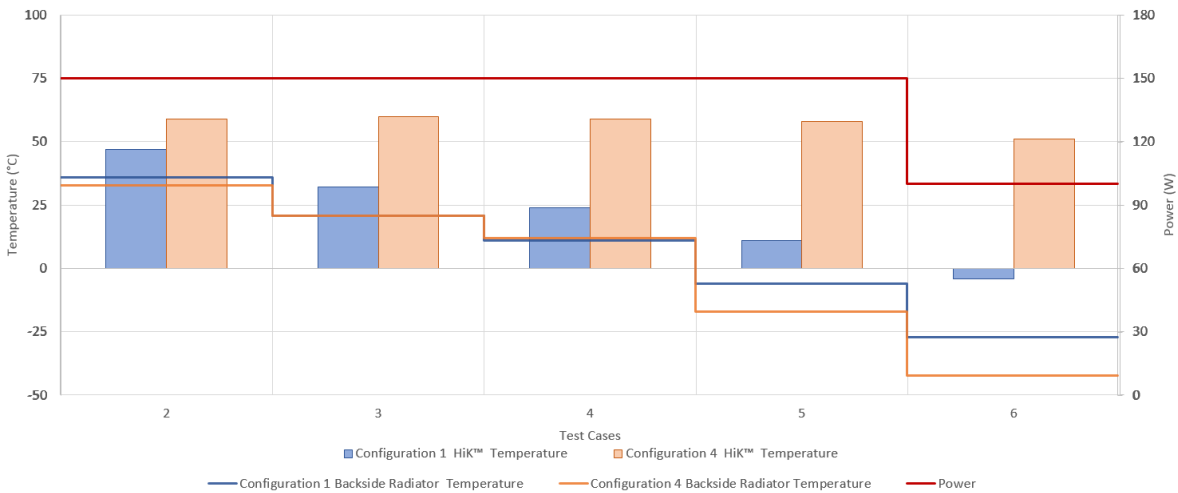


Figure 16: Configuration 1 and 4 HiK™ Temperatures Compared to HiK™ Radiator Temperature and Power for Test Cases 2 through 6

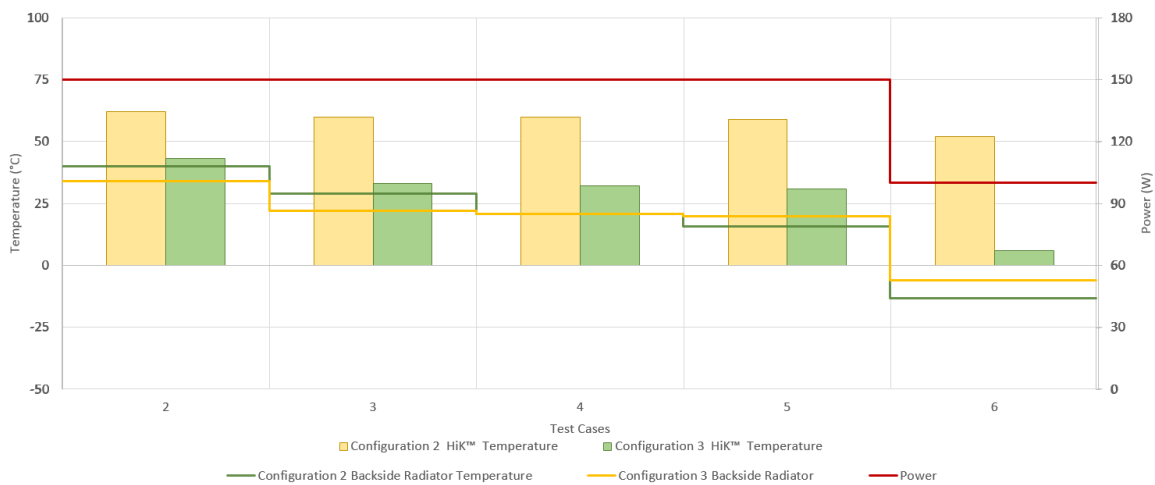


Figure 17: Configuration 2 and 3 HiK™ Temperatures Compared to GCHP Radiator Temperature and Power for Test Cases 2 through 6

Test Case 7 – Survival

For the survival case, the HiK™ plates were maintained to 0°C, the lower limit of the MARE design. The objective of this test was to determine the minimum power required to maintain this operational limit, comparing the novel components and system to the baseline configuration. This test demonstrates the shut down capability of the VCHP and GCHP radiator. The minimum power is also used to calculate the turn down ratio of the system. The variable conductance heat pipe was the driving component during survival conditions in isolating the heat source from the environment, as evidenced in the reduction in Q_{TCS} for configurations including the VCHP, 2 and 4.

Table 5c: Results – Test Case 7

Test Case	7			
Component Q	Configuration			
	1	2	3	4
Q _{in}	115	10	83	9
Q _{in_Radiator}	0	0	0	0
	Percentage (%)			
Q _{TCS}	90	12	87	1
Q _{MLI}	7	63	10	71
Q _{TS}	2	25	3	28
Q _{Radiator}	78	100	90	100
Q _{MLI_Radiator}	22	0	10	0

Supplemental Testing

In addition to the test cases listed above, Configurations 1 and 2 were evaluated for sensitivity to inclination. Given the time constraints, this test could not be performed for Configurations 3 and 4.

Inclination

Configurations 1 and 2 maintained 50°C on the HiK™ plate in nominal (0°), adverse (-4.2°), and aided (+4.2°) gravity inclinations for two hours each. The system was adjusted ± 4.2° from 0° to account for a vehicle design requirement of maintain performance at ± 25° on the lunar surface. The architecture is such that the condenser is always above the evaporator, but the negative inclination of the evaporator created an adverse condition. From this testing, the CCHP in Configuration 1’s dual-bored, grooved wick evaporator was more affected at an adverse inclination than was the VCHP in Configuration 2; the VCHP has a sintered wick evaporator. Configuration 1 had a 31% reduction in power in adverse conditions from nominal compared to a 20% reduction for Configuration 2. The heat transport capability in both Configuration 1 and 2 increased in the gravity aided position.

	Angle of Inclination (°)		
	0	-4.2	+4.2
	System Q (W)		
Q _{HiK_Configuration_1}	295	203	306
Q _{HiK_Configuration_2}	89	71	102

VI. Conclusion

This publication presents all the work performed, from the proposal phase to the proof of concept, of a fully passive thermal management system for a mid-sized lunar lander. This testing successfully demonstrated the initiative to reduce cost and infuse existing research into needed NASA applications by leveraging on existing Small Business Innovation Research (SBIR) contracts. A series of benchtop and component level testing has been performed on the HiK™ plates and hybrid wick VCHPs, including on-orbit operations inside the APTx suite. This publication documents the integration of these technologies in a full system level thermal performance test. The results showed the hybrid VCHP to be the driving component during survival conditions, allowing a reduction of survival heater power of approximately 100 watts compared to the baseline design, Configuration 1. When comparing performance of CCHP systems, Configurations 1 and 3, during the survival conditions, there is a reduction in survival power by

approximately 30 watts when the CCHP is coupled with the GCHP radiator, Configuration 3. However, this may be influenced by radiator sizing; the HiK™ radiator had a front radiative area of 0.697m² compared to the 0.368m² of the GCHP radiator.

In addition, The VCHP provided the tightest temperature control at the heat spreader in cases 2 through 6 when compared to the baseline, Configuration 1, and the GCHP Radiator with the CCHP in Configuration 3.

Addressing the technology gaps identified in the NASA Technology Roadmaps, turn down ratios were evaluated for Configurations 1 and 2. Dividing the maximum power by the minimum power required to maintain MARE operational limits, results for Cases 1 and 7, yielded a turn down ratio for Configuration 1 of 3:1 and a turn down ratio for Configuration 2 of 9:1.

Another way to look at this system level turn down ratio is to assume Q_{Radiator} is the heat load rejected by the full TCS system from HiK™ to thermal link to radiator, accounting for losses. Dividing the maximum Q_{Radiator} by the minimum Q_{Radiator} , results for Cases 1 and 7, yielded a turn down ratio for Configuration 1 of 2:1 and a turndown ratio for Configuration 2 of 50:1.

With the knowledge gained this effort, the team can improve modeling and predictions, refining the fully passive thermal control system for lunar missions and beyond.

Future Work

The thermal math model created will be correlated with the test data and the lunar mission profile will be reassessed in support of lunar lander development efforts. Additional component and system level characterization will be performed and documented in an upcoming publication.

Acknowledgments

The development and assembly of the test articles in this publication was done by the NASA JSC Passive Thermal Technology Development (PTTD) team with the support of a number of JSC NASA interns. We would like to specifically acknowledge the support of Zaida Hernandez, Yuvraj Rathore, Arlene Lopez, Christian Renovato and Ian Marlin. We would also like to give thanks to Mr. Richard Hagen, the Additive Manufacturing Lead at JSC, for his support in the design and manufacturing of the thermal spacers used for the thermal design.

References

¹ NASA Technology Roadmaps , <https://www.nasa.gov/offices/oct/home/roadmaps/index.html>

² https://www.nasa.gov/mission_pages/station/research/experiments/2360.html

³ Ababneh, Mohammed T., Calin Tarau, William G. Anderson, Angel R. Alvarez-Hernandez, Stephania Ortega Jeffery T. Farmer, and Robert Hawkins, “Demonstration of Copper-Water Heat Pipes Embedded in High Conductivity (HiK™) Plates in the Advanced Passive Thermal eXperiment (APT_x) on the International Space Station (ISS)”, *48th International Conference on Environmental Systems*, July,2018.

⁴ Ababneh, Mohammed T., Calin Tarau, William G. Anderson, Angel R. Alvarez-Hernandez, Stephania Ortega Jeffery T. Farmer, and Robert Hawkins, “Advanced Passive Thermal eXperiment (APT_x) for Warm Reservoir Hybrid-Wick Variable Conductance Heat Pipes on the International Space Station (ISS)”, *48th International Conference on Environmental Systems*, July,2018.

⁵ Ababneh, M.T., Tarau, C., Anderson, W.G., Farmer, J.T. and Alvarez-Hernandez, A.R., “Hybrid Heat Pipes for Lunar and Martian Surface and High Heat Flux Space Applications,” *46th International Conference on Environmental Systems*, July, 2016.

⁶ Ababneh, M.T., Tarau, C. and Anderson, W.G., “Hybrid Heat Pipes for Planetary Surface and High Heat Flux Applications,” *45th International Conference on Environmental Systems*, July, 2015.